Transverse Momentum Distributions of Positively Charged Mesons and Light Fragments Produced in Pb-Pb Collisions at 2.76 TeV

Hai-Ling Lao[a], Hua-Rong Wei[a], Fu-Hu Liu[a,1], and Roy A. Lacey[b,2]

[a]*Institute of Theoretical Physics, Shanxi University, Taiyuan, Shanxi 030006, China*
[b]*Departments of Chemistry & Physics, Stony Brook University, Stony Brook, NY 11794, USA*

Abstract: Transverse momentum distributions of positively charged mesons (positive pions π^+ and positive kaons K^+), baryons (protons p), and light fragments (deuterons d and one of helium isotopes ^{3}He) produced in mid-rapidity interval ($|y| < 0.5$) in lead-lead (Pb-Pb) collisions with different centrality intervals, measured by the ALICE Collaboration at center-of-mass energy per nucleon pair $\sqrt{s_{NN}} = 2.76$ TeV, are uniformly and approximately described by the Tsallis statistics. The dependences of parameteres (effective temperature, entropy index, and normalization constant) on centrality and rest mass are obtained. The source temperature and particle transverse (or radial) flow velocity at the kinetic freeze-out of the interacting system are obtained from the relations between effective temperature and rest mass as well as mean transverse momentum and rest mass, respectively.

Keywords: Transverse momentum distribution, source temperature, radial flow velocity

PACS: 25.75.Dw, 24.10.Nz, 24.10.Pa

1 Introduction

High energy nucleus-nucleus (heavy ion) collisions at the large hadron collider (LHC) [1–6] has been providing another excellent environment and condition of high temperature and density, where the new state of matter, namely the quark-gluon plasma (QGP) [7, 8], is expected to form and to live for a longer lifetime than that at the relativistic heavy ion collider (RHIC) [1–3]. Although the RHIC is performed for more abundant collisions, the LHC is run at higher energies. Presently, the LHC has performed three different types of collisions: proton-proton (pp), proton-lead (p-Pb), and lead-lead (Pb-Pb) collisions at different collision energies. The former two are not expected to form the QGP due to small system, though the deconfinement of quarks and gluons may appear. The latter is expected to form the QGP due to large system and high energy.

It is believed that the QGP is formed in Pb-Pb collisions at the LHC and in nucleus-nucleus collisions at lower energy until dozens of GeV at the RHIC [9, 10]. If mesons are

---

[1]E-mail: fuhuliu@163.com; fuhuliu@sxu.edu.cn
[2]E-mail: Roy.Lacey@Stonybrook.edu

produced in the participant region where violent collision had happened and the QGP is formed, nuclear fragments are expected to emit in spectator region where non-violent evaporation and fragmentation had happened. It should be noted that the participant and spectator are concepts of the participant-spectator model [11]. The production mechanisms of mesons and fragments in high energy nucleus-nucleus collisions should be different from each other. The former results from the QGP, and the latter results from the evaporation (light fragments), fragmentation (intermediate fragments), and residual nucleus (the largest fragment). Generally, baryons can be produced in both participant and spectator.

Because nuclear fragments are produced in very forward rapidity region, it is difficult to measure them at colliders due to passing the beam. Instead, nuclear fragments produced in projectile and target have been usually measured in fixed target experiments such as in nuclear emulsion or CR-39 plastic target/detector at accelerators [12, 13]. Fortunately, the ALICE Collaboration [14, 15] measured together the light fragments (deuterons d and one of helium isotopes ^{3}He), positively charged mesons (positive pions π^+ and positive kaons K^+), and baryons (protons p) produced in lead-lead (Pb-Pb) collisions with different centrality intervals at the LHC. It gives us a chance to describe uniformly the three types of final-state products. In particular, we are interested in the uniform description of transverse momentum distributions of π^+, K^+, p, d, and ^{3}He.

More than ten functions are used in the descriptions of transverse momentum distributions. In the present work, we select the Tsallis statistics [16–18] due to its covering the sum of two or three standard distributions [19, 20] and describing temperature fluctuations among different local equilibrium states. Based on the descriptions of the experimental data of the ALICE Collaboration [14, 15] on Pb-Pb collisions at center-of-mass energy per nucleon pair $\sqrt{s_{NN}} = 2.76$ TeV, the source temperature and particle transverse (or radial) flow velocity at the kinetic freeze-out of the interacting system (participant) are obtained from the relations between effective temperature and rest mass as well as mean transverse momentum and rest mass, respectively.

The structure of the present work is as followings. The model and method are shortly described in section 2. Results and discussion are given in section 3. In section 4, we summarize our main observations and conclusions.

2 The model and method

We discuss the collision process in the framework of the multisource thermal model [21–23]. According to the model, many emission sources are formed in participant and spectator [11] in high energy nucleus-nucleus collisions. The particles and fragments are produced in the participant and spectator respectively, where the freeze-out temperature of the participant is expected to be larger than that of the spectator, though the effective temperature extracted from particle spectrum is less than that from fragment spectrum due to mass or flow effect. We can choose different statistics or distributions to describe the emission sources and their particle (fragment) spectra. These statistics or distributions include, but are not limited to, the Tsallis statistics [16–18], the standard (Boltzmann, Fermi-Dirac, and Bose-Einstein) distributions [19], the Tsallis forms of

standard distributions [24–29], the Erlang distribution [21], and so forth.

The Tsallis statistics results in a Tsallis transverse momentum (p_T) distribution which covers two or three standard p_T distributions. The Tsallis forms of standard p_T distributions result in p_T distributions which cover two or three Tsallis p_T distributions [20]. It is needless to choose the standard p_T distributions due to multiple sources (temperatures). It is also needless to choose the Tsallis forms of standard p_T distributions due to not too many sources (temperatures). A middle way is to choose the Tsallis statistics and its p_T distribution which describes the temperature fluctuation in a few local sources to give an average value. These local sources with different excitation degrees can be naturally described by the standard p_T distributions with different effective temperatures.

The Tsallis statistics has more than one function forms [16–18, 24–29]. We consider a simplified form of the joint unit-density function of p_T and rapidity (y) in the Tsallis statistics [18]

$$\frac{d^2N}{dydp_T} = \frac{gV}{(2\pi)^2} p_T \sqrt{p_T^2 + m_0^2} \cosh y \left[1 + \frac{q-1}{T}\left(\sqrt{p_T^2 + m_0^2}\cosh y - \mu\right)\right]^{-q/(q-1)}, \qquad (1)$$

where N is the particle or fragment number, g is the degeneracy factor, V is the volume of the participant or spectator, T is the temperature which describes averagely a few local sources (equilibrium states) in the participant or spectator, q is the entropy index which describes the degree of non-equilibrium among different local states, μ is the chemical potential which is related to $\sqrt{s_{NN}}$ [30] and can be regarded as 0 at the LHC, m_0 is the rest mass of the considered particle. Generally, $gV/(2\pi)^2$ can be regarded as the normalization constant which is related to other parameters.

Eq. (1) results in the transverse momentum distribution as follows

$$f(p_T) = \frac{1}{N}\frac{dN}{dp_T} \propto p_T \sqrt{p_T^2 + m_0^2} \int_{y_{\min}}^{y_{\max}} \cosh y \left[1 + \frac{q-1}{T}\left(\sqrt{p_T^2 + m_0^2}\cosh y - \mu\right)\right]^{-q/(q-1)} dy, \qquad (2)$$

where $y_{\max}$ and $y_{\min}$ denote the maximum and minimum rapidities, respectively. Similarly, Eq. (1) results in the rapidity distribution as follows

$$f(y) = \frac{1}{N}\frac{dN}{dy} \propto \cosh y \int_0^{p_{T\max}} p_T \sqrt{p_T^2 + m_0^2}\left[1 + \frac{q-1}{T}\left(\sqrt{p_T^2 + m_0^2}\cosh y - \mu\right)\right]^{-q/(q-1)} dp_T, \qquad (3)$$

where $p_{T\max}$ denotes the maximum transverse momentum. The validity of Eqs. (2) and (3) is obvious due to Eq. (1).

Further, the momentum (p), energy (E), and kinetic energy (E_{kin}) distributions are

$$f(p) = \frac{1}{N}\frac{dN}{dp} \propto p^2\left[1 + \frac{q-1}{T}\left(\sqrt{p^2 + m_0^2} - \mu\right)\right]^{-q/(q-1)}, \qquad (4)$$

$$f(E) = \frac{1}{N}\frac{dN}{dE} \propto E\sqrt{E^2 - m_0^2}\left[1 + \frac{q-1}{T}\left(E - \mu\right)\right]^{-q/(q-1)}, \qquad (5)$$

and

$$f(E_{kin}) = \frac{1}{N}\frac{dN}{dE_{kin}} \propto \left(E_{kin} + m_0\right)\sqrt{E_{kin}^2 + 2m_0E_{kin}}\left[1 + \frac{q-1}{T}\left(E_{kin} + m_0 - \mu\right)\right]^{-q/(q-1)}, \qquad (6)$$
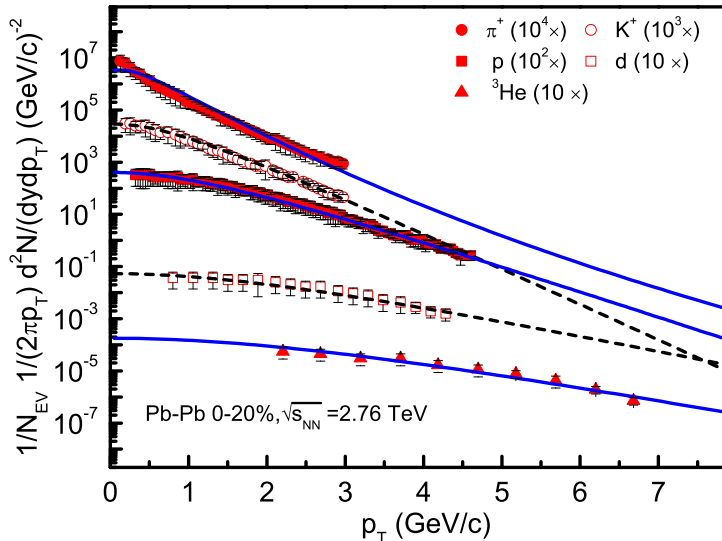
3

Figure 1. Transverse momentum distributions of π^+, K^+, p, d, and ^{3}He produced in mid-rapidity interval ($|y| < 0.5$) in Pb-Pb collisions at $\sqrt{s_{NN}} = 2.76$ TeV. The symbols represent the experimental data of the ALICE Collaboration [15] in centrality interval 0–20%, which are scaled by different amounts marked in the panel. The curves are our results fitted by using the Tsallis p_T distribution and the method of least squares.

respectively. Based on Eq. (2) and a Monte Carlo calculation, the validity of Eq. (4) can be checked by $p = p_T/\sin\theta$ and the isotropic assumption for an emission source, where θ denotes the emission angle of the considered particle (fragment). The validity of Eqs. (5) and (6) can be checked by $E^2 = p^2 + m_0^2$ and $|f(p)dp| = |f(E)dE|$ based on Eq. (4), as well as $E = E_{kin} + m_0$ and $|f(E)dE| = |f(E_{kin})dE_{kin}|$ based on Eq. (5), respectively.

3 Results and discussion

Figure 1 presents the transverse momentum distributions, $(1/N_{EV})d^2N/(2\pi p_T dy dp_T)$, of π^+, K^+, p, d, and ^{3}He produced in mid-rapidity interval ($|y| < 0.5$) in Pb-Pb collisions at $\sqrt{s_{NN}} = 2.76$ TeV, where N_{EV} denotes the number of events. The symbols represent the experimental data of the ALICE Collaboration [15] in centrality interval 0–20%, which are scaled by different amounts marked in the panel. The curves are our results fitted by using the Tsallis p_T distribution and the method of least squares. The values of related parameters, T, q, and N_0 (the normalization constant which is used to compare the normalized curve with experimental data), are listed in Table 1 with values of χ^2 per degree of freedom (χ^2/dof). One can see that the Tsallis p_T distribution describes uniformly and approximately π^+, K^+, p, d, and ^{3}He spectra. The effective temperature increases with increase of particle (fragment) mass.

Table 1. Values of T, q, N_0, and χ^2/dof corresponding to the curves in Figures 1–3.
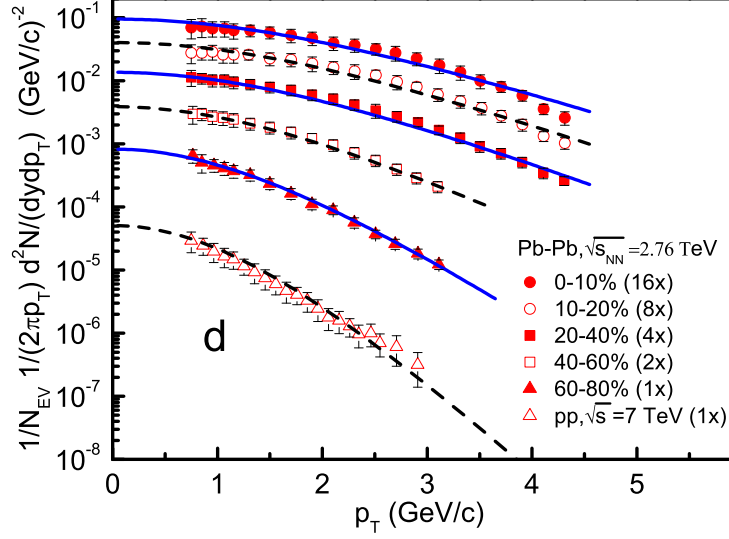
Figure 2. The same as for Figure 1, but showing the results of d in Pb-Pb collisions with different centrality intervals and in pp collisions.

Figure	Type	T (GeV)	q	N_0	χ^2/dof
Figure 1	π^+	0.190 ± 0.013	1.0380 ± 0.0208	200.000 ± 20.000	3.689
	K^+	0.297 ± 0.027	1.0010 ± 0.0200	23.400 ± 3.510	1.695
	p	0.410 ± 0.037	1.0010 ± 0.0170	4.620 ± 0.693	0.191
	d	0.650 ± 0.072	1.0010 ± 0.0200	0.010 ± 0.003	0.166
	^{3}He	0.720 ± 0.058	1.0013 ± 0.0160	$(4.000 \pm 0.600) \times 10^{-5}$	2.723
Figure 2	0–10%	0.700 ± 0.050	1.0010 ± 0.0070	$(1.188 \pm 0.107) \times 10^{-2}$	1.425
	10–20%	0.650 ± 0.030	1.0010 ± 0.0040	$(9.500 \pm 0.950) \times 10^{-3}$	0.797
	20–40%	0.600 ± 0.030	1.0010 ± 0.0190	$(6.000 \pm 0.780) \times 10^{-3}$	0.604
	40–60%	0.490 ± 0.105	1.0010 ± 0.0140	$(2.950 \pm 0.220) \times 10^{-3}$	0.011
	60–80%	0.355 ± 0.079	1.0010 ± 0.0100	$(1.000 \pm 0.007) \times 10^{-3}$	1.731
	pp	0.255 ± 0.013	1.0010 ± 0.0009	$(5.000 \pm 0.650) \times 10^{-5}$	1.757
Figure 3	0–20%	0.680 ± 0.054	1.0040 ± 0.0030	$(6.100 \pm 0.793) \times 10^{-6}$	1.127
	20–80%	0.750 ± 0.016	1.0005 ± 0.0004	$(3.000 \pm 0.390) \times 10^{-5}$	0.929

Figure 2 is similar to Figure 1, but it shows the results of d in different centrality intervals, which are scaled by different amounts marked in the panels. At the same time, the result in pp collisions at $\sqrt{s} = 7$ TeV is presented for comparison, where $\sqrt{s}$ is a simplified form of $\sqrt{s_{NN}}$ for pp collisions. Figure 3 is similar to Figure 1, too, but it shows the results of ^{3}He in centrality intervals 0–20% and 20–80%. The related parameter values are listed in Table 1 with values of χ^2/dof. One can see that the Tsallis statistics describes approximately the experimental data of light fragments produced in Pb-Pb collisions with different centrality intervals at the LHC. The effective temperature extracted from d spectra decreases with decrease of centrality (or increase of centrality
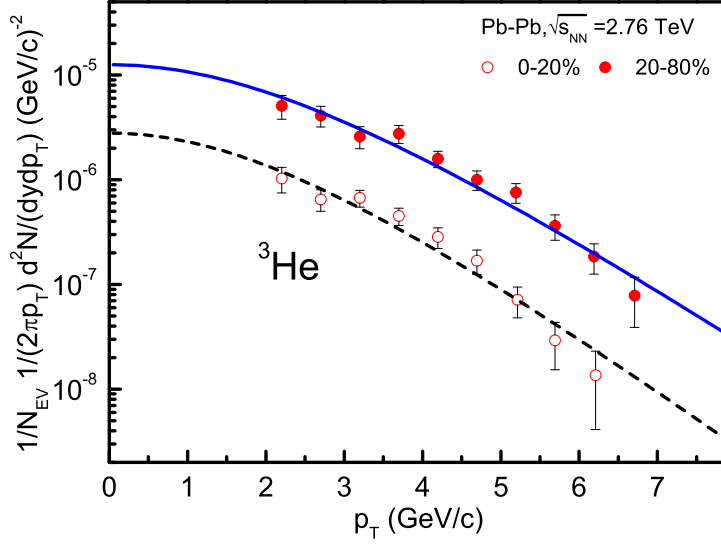
5

Figure 3. The same as for Figure 1, but showing the results of ^{3}He in Pb-Pb collisions with two centrality intervals.

percentage).

To study the change trends of parameters with centrality interval (C) of event and rest mass of particle, Figure 4 gives the dependences of (a) T on C for d in events with different centrality intervals and (b) T on m_0 for particles and fragments in events with centrality interval 0–20%. The symbols represent the parameter values listed in Table 1 and the curves are our results fitted by the method of least squares. The curve in Figure 4(a) is described by

$$T = -(0.000050 \pm 0.000002)C^2 - (0.0015 \pm 0.0001)C + (0.692 \pm 0.001) \qquad (7)$$

with χ^2/dof=0.109, where T is in the units of GeV. The solid, dotted, and dashed curves in Figure 4(b) are linear fittings for i) π^+, K^+, and p; ii) π^+, K^+, p, and d; and iii) π^+, K^+, p, d, and ^{3}He, which are described by

$$T = (0.155 \pm 0.006) + (0.275 \pm 0.010)m_0, \qquad (8)$$

$$T = (0.160 \pm 0.005) + (0.264 \pm 0.005)m_0, \qquad (9)$$

and

$$T = (0.199 \pm 0.036) + (0.204 \pm 0.022)m_0, \qquad (10)$$

with χ^2/dof=0.130, 0.160, and 3.294, respectively, where m_0 is in the units of GeV/c^2. The intercept in Eq. (8) is regarded as the kinetic freeze-out temperatures [31–34] of the participant region, which is 0.155 GeV corresponding to massless particles. Including ^{3}He causes an abnormal large intercept. Except for the mass or flow effect, mesons and fragments should not be included in the same $T - m_0$ relation due to they being produced

in participant and spectator respectively. The blast-wave model [35] gives the kinetic freeze-out temperature extracted from d spectra to be 0.077–0.124 GeV and from ^{3}He spectra to be 0.101 GeV [15] which is less than the present work. In particular, the blast-wave model gives the kinetic freeze-out temperature in central collisions to be less than that in peripheral collisions [15], which is inconsistent to Figure 4(a) which shows an opposite result.

In Figure 5, the dependences of (a) q on C for d in events with different centrality intervals and (b) q on m_0 for particles and fragments in events with centrality interval 0–20% are given. The symbols represent the parameter values listed in Table 1. For d in events with different centrality intervals, the values of q are the same with different uncertainties, which are also shown by the horizontal line in the panel [Figure 5(a)]. For the events with centrality interval 0–20%, π^+ corresponds to a larger q than others which show almost the same q with different uncertainties [Figure 5(b)]. Because of all values of q being small, the interacting system stays approximately in an equilibrium state.

In Figure 6, the dependences of (a) N_0 on C for d in events with different centrality intervals and (b) N_0 on m_0 for particles and fragments in events with centrality interval 0–20% are given. The symbols represent the parameter values listed in Table 1. The curves are our results fitted by the method of least squares, which are described by

$$N_0 = (0.016 \pm 0.001) \exp[-(0.030 \pm 0.002)C] - (0.0010 \pm 0.0001) \tag{11}$$

and

$$N_0 = (547.849 \pm 71.220) \exp[-(5.809 \pm 0.116)m_0] \tag{12}$$

with $\chi^2/$dof=1.677 and 7.017 respectively. It is shown that N_0 decreases with decrease of centrality. The larger the particle (fragment) mass is, the lower the production probability is. The large $\chi^2/$dof for Eq. (12) is explained due to small errors in N_0

To extract the radial flow velocity, we display the dependence of mean transverse momentum ($\langle p_T \rangle$) on m_0 in Figures 7. The symbols represent the values of $\langle p_T \rangle$ for different particles (fragments) calculated according to the Tsallis p_T distribution. The solid, dotted, and dashed curves in Figures 7 are linear fittings for i) π^+, K^+, and p; ii) π^+, K^+, p, and d; and iii) π^+, K^+, p, d, and ^{3}He, which are described by

$$\langle p_T \rangle = (0.305 \pm 0.007) + (0.491 \pm 0.011)m_0, \tag{13}$$

$$\langle p_T \rangle = (0.294 \pm 0.009) + (0.517 \pm 0.008)m_0, \tag{14}$$

and

$$\langle p_T \rangle = (0.347 \pm 0.049) + (0.435 \pm 0.031)m_0, \tag{15}$$

with $\chi^2/$dof=0.050, 0.124, and 0.970, respectively, where $\langle p_T \rangle$ is in the units of GeV/c. From the consideration of dimension, the slope in Eq. (13) is regarded as the (average) radial flow velocity, which is close to $0.5c$. Including d and ^{3}He cause a small effect for the radial flow velocity. Because mesons and fragments should not be included in the same $\langle p_T \rangle - m_0$ relation. Eqs. (14) and (15) are not accurate. The blast-wave model [35] gives the radial flow velocity for d is 0.38–0.63c and for ^{3}He is 0.56–0.57c [15] which is comparable with the present work.
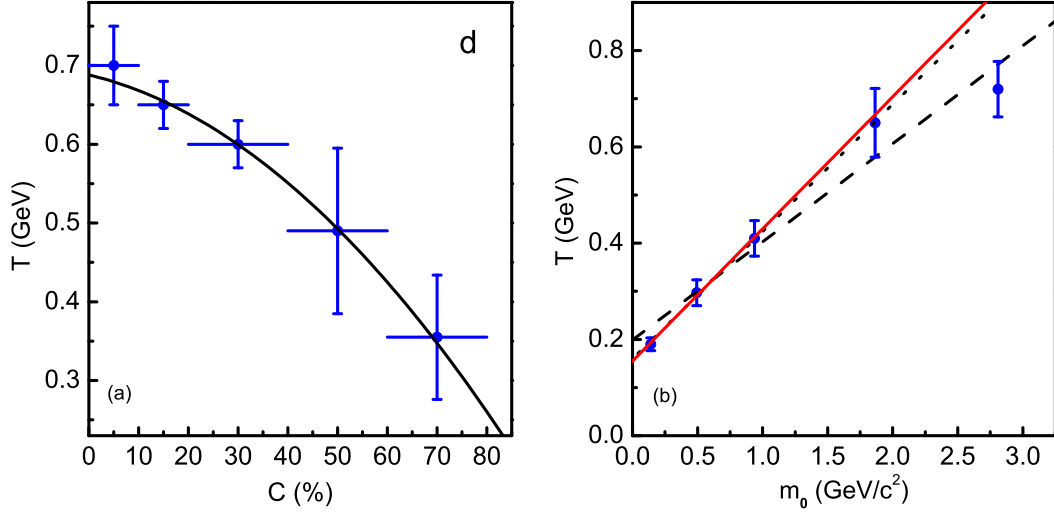
Figure 4. Dependence of (a) T on C for d in events with different centrality intervals and (b) T on m_0 for particles and fragments in events with centrality interval 0–20%. The symbols represent the parameter values listed in Table 1 and the curves are our results fitted by the method of least squares.
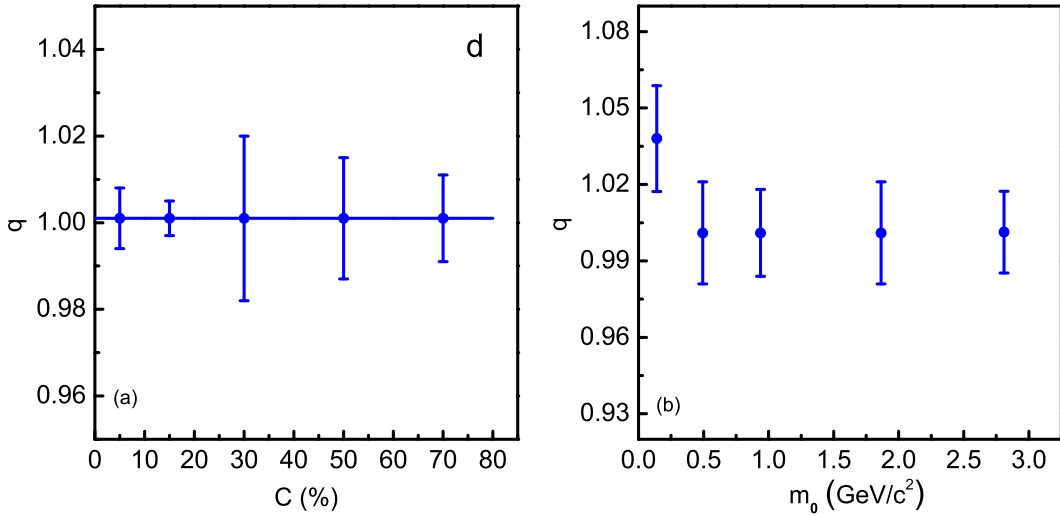

Figure 5. Dependence of (a) q on C for d in events with different centrality intervals and (b) q on m_0 for particles and fragments in events with centrality interval 0–20%. The symbols represent the parameter values listed in Table 1. The horizontal line in Figure 5(a) indicates the same value of q with different uncertainties.
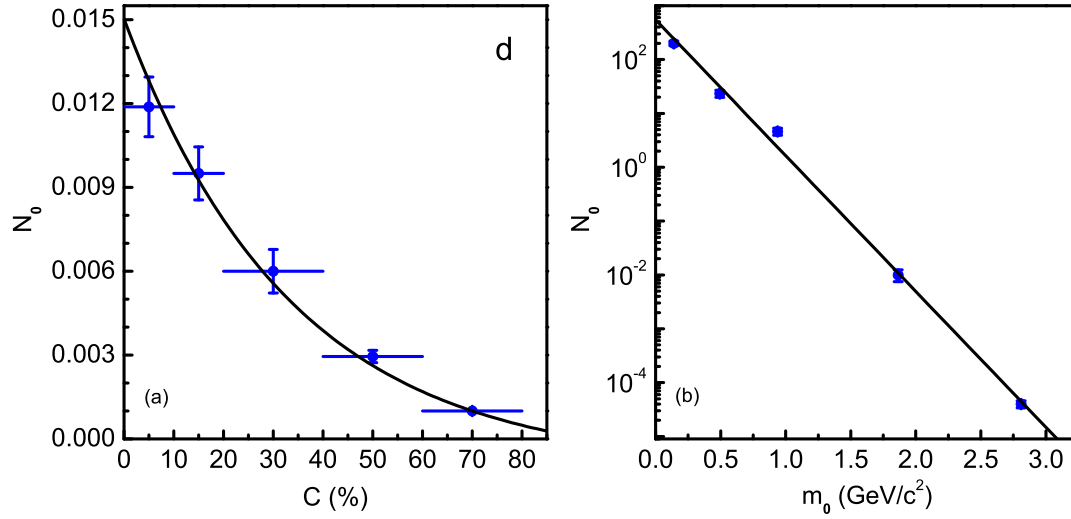
8

Figure 6. Dependence of (a) N_0 on C for d in events with different centrality intervals and (b) N_0 on m_0 for particles and fragments in events with centrality interval 0–20%. The symbols represent the parameter values listed in Table 1. The curve and line are our results fitted by the method of least squares.
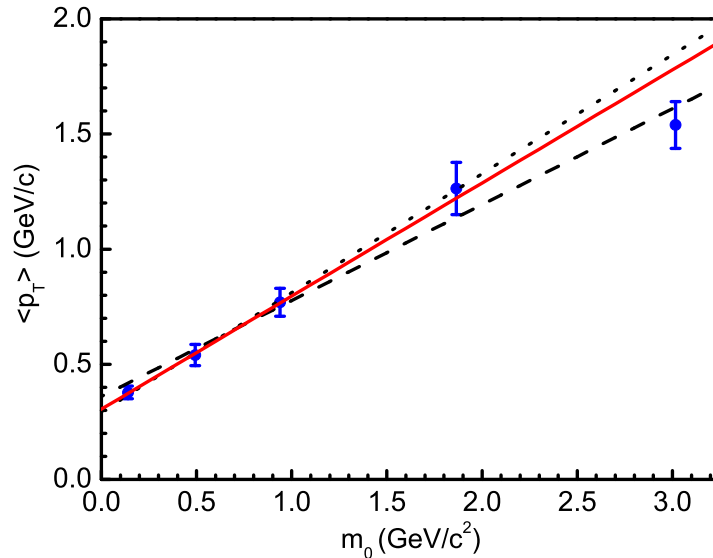

Figure 7. Dependence of $\langle p_T \rangle$ on m_0 for particles and fragments in events with centrality interval 0–20%. The symbols represent the values of $\langle p_T \rangle$ calculated according to the Tsallis p_T distribution. The curves are our results fitted by the method of least squares.

9

4   Conclusions

We summarize here our main observations and conclusions.

(a) The transverse momentum distributions of π^+, K^+, p, d, and ^{3}He produced in Pb-Pb collisions with different centrality intervals at the LHC are uniformly analyzed by using the Tsallis statistics. The results calculated by us can fit approximately the experimental data of the ALICE Collaboration. The values of parameters such as the effective temperature, entropy index, and normalization constant are obtained.

(b) The effective temperature extracted from transverse momentum spectra increases with increase of particle (fragment) mass, and decreases with decrease of centrality. The kinetic freeze-out temperature of the participant region in central collisions extracted from the intercept in the relation between effective temperature and rest mass is 0.155 GeV. The mass effect for ^{3}He causes a large departure from the kinetic freeze-out temperature.

(c) The radial flow velocity extracted from the slope in the relation between mean transverse momentum and rest mass is close to $0.5c$. The method for extraction of the kinetic freeze-out temperature and radial flow velocity used in the present work is different from the blast-wave model. Both the methods give different results in some cases such as for kinetic freeze-out temperature, and comparable results in other cases such as for radial flow velocity.

References

[1] J. Uphoff, O. Fochler, Z. Xu, and C. Greiner, "Open heavy flavor at RHIC and LHC in a partonic transport model," *Acta Physica Polonica B Proceedings Supplement*, vol. 5, no. 2, pp. 555–560, 2012.

[2] Y. Zhong, C.-B. Yang, X. Cai, and S.-Q. Feng, "A systematic study of magnetic field in relativistic heavy-ion collisions in the RHIC and LHC energy regions," *Advances in High Energy Physics*, vol. 2015, Article ID 193039, 10 pages, 2015.

[3] S. Chatterjee, S. Das, L. Kumar, D. Mishra, B. Mohanty, R. Sahoo, and N. Sharma, "Freeze-out parameters in heavy-ion collisions at AGS, SPS, RHIC, and LHC energies," *Advances in High Energy Physics*, vol. 2015, Article ID 349013, 20 pages, 2015.

[4] R. Preghenella (for the ALICE Collaboration), "Identified-particle production and spectra with the ALICE detector in pp and Pb-Pb collisions at the LHC," *Acta Physica Polonica B*, vol. 43, no. 4, pp. 555–562, 2012.

[5] R. C. Hwa, "Recognizing critical behavior amidst minijets at the Large Hadron Collider," *Advances in High Energy Physics*, vol. 2015, Article ID 526908, 10 pages, 2015.

[6] G.-L. Ma and M.-W. Nie, "Properties of full jet in high-energy heavy-ion collisions from parton scatterings," *Advances in High Energy Physics*, vol. 2015, Article ID 967474, 12 pages, 2015.

[7] N. Itoh, "Hydrostatic equilibrium of hypothetical quark stars," *Progress in Theoretical Physics*, vol. 44, no. 1, pp. 291–292, 1970.

[8] T. D. Lee and G. C. Wick, "Vacuum stability and vacuum excitation in a spin-0 field theory," *Physical Review D*, vol. 9, no. 8, pp. 2291–2316, 1974.

[9] R. A. Lacey, "Indications for a critical end point in the phase diagram for hot and dense nuclear matter," *Physical Review Letters*, vol. 114, no. 14, Article ID 142301, 5 pages, 2015.

[10] M. Nasim, V. Bairathi, M. K. Sharma, B. Mohanty, and A. Bhasin, "A review on ϕ meson production in heavy-ion collision," *Advances in High Energy Physics*, vol. 2015, Article ID 197930, 16 pages, 2015.

[11] R. J. Glauber, "High-energy collision theory," in *Lectures of Theoretical Physics*, W. E. Brittin and L. G. Dunham, Eds., vol. 1, pp. 315–414, Interscience, New York, NY, USA, 1959.

[12] M. I. Adamovich, M. M. Aggarwal, Y. A. Alexandrov et al. (EMU01 Collaboration),"Angular distributions of light projectile fragments in deep inelastic Pb+Em interactions at 160A GeV," *The European Physical Journal A*, vol. 6, no. 4, pp. 421–425, 1999.

[13] P. B. Price and Y. D. He, "Behavior of nuclear projectile fragments produced in collisions of 14.5A GeV ^{28}Si with Pb and Cu targets," *Physical Review C*, vol. 43, no. 2, pp. 835–848, 1991.

[14] F. Barile (for the ALICE Collaboration), "Light (hyper-)nuclei production at the LHC measured with ALICE," in *Proceedings of 3rd International Conference on New Frontiers in Physics*, Kolymbari, Crete, Greece, 28 July – 6 August, 2014.

[15] J. Adam, D. Adamová, M. M. Aggarwal et al. (ALICE Collaboration), "Production of light nuclei and anti-nuclei in pp and Pb-Pb collisions at LHC energies," Preprint CERN-PH-EP-2015-025, http://arxiv.org/abs/1506.08951, 2015.

[16] C. Tsallis, "Possible generalization of Boltzmann-Gibbs statistics," *Journal of Statistical Physics*, vol. 52, no. 1-2, pp. 479–487, 1988.

[17] T. S. Biró, G. Purcsel, and K. Ürmössy, "Non-extensive approach to quark matter," *The European Physical Journal A*, vol. 40, no. 3, pp. 325–340, 2009.

[18] J. Cleymans and D. Worku, "Relativistic thermodynamics: transverse momentum distributions in high-energy physics," *The European Physical Journal A*, vol. 48, Article ID 160, 8 pages, 2012.

[19] P. Z. Ning, L. Li, and D. F. Min, *Foundation of Nuclear Physics: Nucleons and Nuclei*, Higher Education Press, Beijing, China, 2003.

[20] F.-H. Liu, Y.-Q. Gao, and H.-R. Wei, "On descriptions of particle transverse momentum spectra in high energy collisions," *Advances in High Energy Physics*, vol. 2014, Article ID 293387, 12 pages, 2014.

[21] F.-H. Liu, Y.-Q. Gao, T. Tian, and B.-C. Li, "Unified description of transverse momentum spectrums contributed by soft and hard processes in high-energy nuclear collisions," *The European Physical Journal A*, vol. 50, no. 6, Article ID 94, 9 pages, 2014.

[22] F.-H. Liu and J.-S. Li, "Isotopic production cross section of fragments in ^{56}Fe+p and ^{136}Xe(^{124}Xe)+Pb reactions over an energy range from $300A$ to $1500A$ MeV," *Physical Review C*, vol. 78, no. 4, Article ID 044602, 13 pages, 2008.

[23] F.-H. Liu, "Unified description of multiplicity distributions of final-state particles produced in collisions at high energies," *Nuclear Physics A*, vol. 810, nos. 1–4, pp. 159–172, 2008.

[24] F. Büyükkiliç and D. Demirhan, "A fractal approach to entropy and distribution functions," *Physics Letters A*, vol. 181, no. 1, pp. 24–28, 1993.

[25] J.-C. Chen, Z.-P. Zhang, G.-Z. Su, L.-X. Chen, and Y.-G. Shu, "q-generalized Bose-Einstein condensation based on Tsallis entropy," *Physics Letters A*, vol. 300, no. 1, pp. 65–70, 2002.

[26] J. M. Conroy and H. G. Miller, "Color superconductivity and Tsallis statistics," *Physical Review D*, vol. 78, no. 5, Article ID 054010, 5 pages, 2008.

[27] F. Pennini, A. Plastino, and A. R. Plastino, "Tsallis entropy and quantal distribution functions," *Physics Letters. A*, vol. 208, nos. 4–6, pp. 309–314, 1995.

[28] A. M. Teweldeberhan, A. R. Plastino, and H. G. Miller, "On the cut-off prescriptions associated with power-law generalized thermostatistics," *Physics Letters A*, vol. 343, nos. 1–3, pp. 71–78, 2005.

[29] J. M. Conroy, H. G. Miller, and A. R. Plastino, "Thermodynamic consistency of the q-deformed Fermi-Dirac distribution in nonextensive thermostatics," *Physics Letters A*, vol. 374, no. 45, pp. 4581–4584, 2010.

[30] A. Andronic, P. Braun-Munzinger, and J. Stachel, "The horn, the hadron mass spectrum and the QCD phase diagram – the statistical model of hadron production in central nucleus-nucleus collisions," *Nuclear Physics A*, vol. 834, nos. 1–4, pp. 237c–240c, 2010.

[31] U. W. Heinz, "Concepts of heavy-ion physics," *Lecture Notes for Lectures Presented at the 2nd CERN – Latin-American School of High-Energy Physics*, San Miguel Regla, Mexico, June 1-14, 2003, http://arxiv.org/abs/hep-ph/0407360, 2004.

[32] S. S. Adler, S. Afanasiev, C. Aidala et al. (PHENIX Collaboration), "Identified charged particle spectra and yields in Au+Au collisions at $\sqrt{s_{NN}} = 200$ GeV," *Physical Review C*, vol. 69, no. 3, Article ID 034909, 32 pages, 2004.

[33] S. Takeuchi, K. Murase, T. Hirano, P. Huovinen, and Y. Nara, "Effects of hadronic rescattering on multistrange hadrons in high-energy nuclear collisions," *Physical Review C*, vol. 92, no. 4, Article ID 044907, 12 pages, 2015.

[34] R. Russo, "Measurement of D^+ meson production in p-Pb collisions with the ALICE detector," Ph.D. thesis, Universitaâ degli Studi di Torino, Italy, 2015, http://arxiv.org/abs/1511.04380, 2015.

[35] E. Schnedermann, J. Sollfrank, and U. W. Heinz, "Thermal phenomenology of hadrons from 200A GeV S+S collisions," *Physical Review C*, vol. 48, no. 5, pp. 2462–2475, 1993.